This is a repository copy of *A refined sin hyperbolic shear deformation theory for sandwich FG plates by enhanced meshfree with new correlation function*.

White Rose Research Online URL for this paper:
http://eprints.whiterose.ac.uk/158865/

Version: Accepted Version

A refined sin hyperbolic shear deformation theory for sandwich FG plates by enhanced meshfree with new correlation function

Tan-Van Vu · Jose L. Curiel-Sosa · Tinh Quoc Bui

Abstract The moving Kriging interpolation-based (MKI) meshfree method is extended to mechanical behavior analysis of isotropic and sandwich functionally graded material plates. The MKI meshfree method, which is free of shear correction factors effect in plate analysis, is further enhanced by introducing a new multi-quadric correlation function, eliminating drawbacks of its conventional form, gaining accurate solution. In this paper, a new refined sin hyperbolic shear deformation plate theory (N-RSHSDT) is introduced for plate kinematics. The present theory gives rise to four governing equations only, and achieves the sin hyperbolic distribution of the transverse shear strains through the plate thickness. To show the accuracy and effectiveness of the developed method, numerical experiments are performed for both isotropic and sandwich composite plates.

Keywords Sandwich plates · Functionally graded materials · Meshfree · Hyperbolic shear deformation theory · Moving Kriging interpolation

T.-V. Vu (✉)
Department of Civil Engineering, University of Architecture Ho Chi Minh City, 196 Pasteur, District 3, Ho Chi Minh City 70000, Vietnam
e-mail: van.vutan@uah.edu.vn

J. L. Curiel-Sosa
Department of Mechanical Engineering, University of Sheffield, Sir Frederick Mappin, Mappin St, Sheffield, UK

T. Q. Bui (✉)
Institute for Research and Development, Duy Tan University, Da Nang City, Vietnam
e-mail: buiquoctinh@duytan.edu.vn;
bui.t.aa@m.titech.ac.jp

T. Q. Bui
Department of Civil and Environmental Engineering, Tokyo Institute of Technology, 2-12-1-W8-22, Ookayama, Meguro-ku, Tokyo 152-8552, Japan

1 Introduction

The objective of the present work is to develop a simple and effective computational approach for the investigation of static bending, natural frequency, and buckling modes of both sandwich functional composite plates and isotropic functional graded plates. The model being presented here combines the moving Kriging interpolation method (MKI) and a new refined sin hyperbolic shear deformation plate theory (N-RSHSDT). The N-RSHSDT theory gives rise to four governing equations only, and does not require the shear correction factors. The distribution of the transverse shear strains through the plate thickness are hence proposed by the sin hyperbolic function, better representing the transverse shear strains. Another objective of the present work is to improve the performance of the conventional MKI in modelling plate problems. As stated in the previous works

by the present authors (Bui et al. 2009, 2011), the conventional MKI inherently owns some drawbacks as its shape functions are significantly affected by the chosen correlation functions. It implies that the widely used Gaussian function, which depends on the so-called correlation function, greatly influences the quality of the MKI shape functions, altering the final solutions of the problems of interest. In fact, this issue has already been analysed and discussed in the previous contributions (Bui et al. 2009, 2011; Bui and Nguyen 2011), and basically it is difficult to appropriately determine a correlation parameter which is applicable for any problems. As indicated in Bui et al. (2009), Bui and Nguyen (2011) the correlation parameter does not have any relation to the physical aspects of the problems. Neither analytical expressions nor theoretical rules are available for determining the optimal values of such correlation variable. In practice, it is often determined through numerical experiments, and it seems that the parameter is problem-dependent. Therefore, in this paper, the MKI is further enhanced by getting rid of such correlation parameter. Instead, we introduce here a new multi-quadric correlation function, which is completely independent on the correlation parameter, eliminating the aforementioned strong effects on the solution. The developed computational framework is then applied to solve static bending, natural frequency, and buckling modes of isotropic plates as well as sandwich composite plates. We thus conduct the numerical experiments to show the accuracy and performance of the proposed approach.

Sandwich plates are a special structure of laminates, which have been widely used in a variety of engineering applications, especially in civil engineering, aerospace, and auto-mobiles, due to their outstanding characteristics. Some excellent features of sandwich structures are, for instance, the bending rigidity, the low specific strength and excellent vibration performance. Sandwich plates are often fabricated where the inner layers are designed to be thicker and those compose of more flexible materials (Bui and Nguyen 2011; Ha 1990). In this work, we particularly consider two types of sandwich plates. The first sandwich plates consist of a single core, which is made by FGM, bonded to two stiff facings by isotropic materials. On the contrary, the second type of sandwich plates consist of a single isotropic core bonded to two stiff facings made by FGM. The detailed description of these two types of sandwich plates is given in the subsequent sections. The considerable advantages gained by the FGM over conventional constituent materials are obvious, and have been widely addressed in the literature. One of the reasons for use of the FGM as the core or the facing sheets in terms of sandwich plates is to reduce or alleviate the material discontinuity among layers. Stress distributions through those layers are smooth, not discontinuous, which is a critical issue, and are found in common conventional layered structures (Do et al. 2017; Yaghoobi and Yaghoobi 2013; Neves et al. 2012; Bessaim et al. 2013).

Meshfree methods have been proved to be an effective numerical technique, which have been introduced and developed for the last few decades, see e.g. (Bui et al. 2009, 2011; Bui and Nguyen 2011; Vu et al. 2017; Sadamoto et al. 2017) and references therein. The application of the meshfree methods to engineering problems has become popular nowadays. The advantages of meshfree methods over traditional mesh-based methods, e.g., the finite element method (FEM), are well-known (Chen et al. 2017). The popular application of the FEM to engineering problem is clear, however its meshing issue is still challenging. In that sense, meshfree methods show great advantages as meshing is no longer required (Vu et al. 2017; Chen et al. 2017; Bui et al. 2016). In general, there are several versions of meshfree methods available in the literature. However, most meshfree methods require a special treatment of the essential boundary conditions, for instance, the moving least square method, where the imposition of the essential boundary condition must be carried out in the sense that the Kronecker delta property is automatically passed. In this context, the MKI does better performance as it is automatically satisfied the Kronecker delta function. Hence, the imposition of the essential boundary condition is treated exactly the same as the conventional FEM (Bui et al. 2009, 2011, 2016; Bui and Nguyen 2011; Vu et al. 2017; Sadamoto et al. 2017).

In summary, the novelties of the present contribution lie in the development of an effective and simple computational approach as per the following features. A new multi-quadric correlation functions is presented to construct MKI shape functions so that the underlying solution becomes stable. A four variable refined plate formulation is derived using a new sin hyperbolic distribution function of the transverse shear strains for

isotropic FGM and sandwich FGM plates, saving computational cost. The present formulation is insensitive to shear locking for thin plate case. We demonstrate the desirable characteristics of the proposed computational approach through numerical experiments by analyzing their mechanical behavior, i.e., static bending, natural frequency, and buckling modes, of sandwich FGM and isotropic FGM plates.

We structure the rest of the paper as follows. A brief review of the isotropic and sandwich FG plates is given in Sect. 2, followed by the formulation of the N-RSHSDT. Meshfree formulation for bending, free vibration and buckling analyses of plates is presented in Sect. 3. Numerical validations and discussions are presented in Sect. 4. Some conclusions drawn from the study are given in Sect. 5.

2 Theoretical formulation

2.1 Functionally graded material plates

Consider a rectangular FGM plate with co-ordinates x, y along its width a, length b and z across its thickness h direction as shown in Fig. 1a. The Cartesian coordinate system attached to the FGM plate, where the xy-plane is coincident with the geometrical midplane of the plate, while the z-axis passed through the centre of the plate. The FGM plate material of young's modulus $E(z)$ and mass density $\rho(z)$ are assumed to be varied only in the plate's thickness direction according to a certain distribution, while Poisson's ratio v is assumed to be constant for simplicity. In this study, three types of functionally graded material (FGM) plates typically consist of isotropic plates (type-A), sandwich plates using with FG material core and isotropic skins (type-B) and vice versa (type-C) are employed for analysing the static bending, natural frequency, and compression buckling.

2.1.1 Type A: isotropic FGM plate

In this case, the FGM plate has the bottom and top faces assumed to be fully metallic and ceramic, respectively. FGM effective material properties of young's modulus $E(z)$ and mass density $\rho(z)$ are computed by a power-law distribution with Voigh's rule of mixtures as follows

$$
\begin{aligned}
E(z) &= E_m + (E_c - E_m)V_c(z) \\
\rho(z) &= \rho_m + (\rho_c - \rho_m)V_c(z)
\end{aligned} \qquad (1a, b)
$$

where the subscripts m, c refer to the metallic and ceramic constituents, respectively; $V_c(z) = (0.5 + z/h)^n$ is the volume fraction of the ceramic, and n is the volume fraction exponent, which governs the gradient index. In this regard, the variation in the ceramic volume $V_c(z)$ with respect to the thickness ratio z/h for different values of the gradient index n (Vu et al. 2017) as show in Fig. 1b.

2.1.2 Type B: sandwich plate with FGM core and isotropic face sheets

In this case, the sandwich FGM plate made by the power-law FGM core and homogeneous face sheets is depicted in Fig. 2a. The volume fraction is assumed to follow as Li et al. (2008)

$$
\begin{aligned}
V_c^{(1)}(z) &= 0, & z &\in [z_1, z_2] \\
V_c^{(2)}(z) &= \left(\frac{z - z_2}{z_3 - z_2}\right)^n, & z &\in [z_2, z_3] \\
V_c^{(3)}(z) &= 1, & z &\in [z_3, z_4]
\end{aligned} \qquad (2a, b, c)
$$

In which $V_c^{(i)}, (i = 1, 2, 3)$ denotes the volume fraction function of layer i; and $(z_3 - z_2)$ is the thickness of core.

2.1.3 Type C: sandwich plates with isotropic core and FGM face sheets

Figure 2b shows the composition of the sandwich FGM plate-type C which has an isotropic core. Two face sheets have metal-rich at surfaces $z = z_1, z = z_4$, and ceramic-rich at surfaces $z = z_2, z = z_3$. In this case, the volume fraction of the ceramic and metal in the face sheets can be expressed as Li et al. (2008)

$$
\begin{aligned}
V_c^{(1)}(z) &= \left(\frac{z - z_1}{z_2 - z_1}\right)^n & z &\in [z_1, z_2] \\
V_c^{(2)}(z) &= 1 & z &\in [z_2, z_3] \\
V_c^{(3)}(z) &= \left(\frac{z_4 - z}{z_4 - z_3}\right) & z &\in [z_3, z_4]
\end{aligned} \qquad (3a, b, c)
$$

wherein $(z_2 - z_1)$ and $(z_4 - z_3)$ is the thickness of the bottom and top face sheets, respectively. The thickness index of each layer of bottom/core/top is indicated as different ratios of $[(z_4 - z_3)/(z_3 - z_2)/(z_2 - z_1)]$.

Fig. 1 **a** Geometry notation and coordinates of an FG plate, **b** variation of ceramic volume fraction $V_c(z)$ with respect to the thickness ratio z/h for different values of the index n
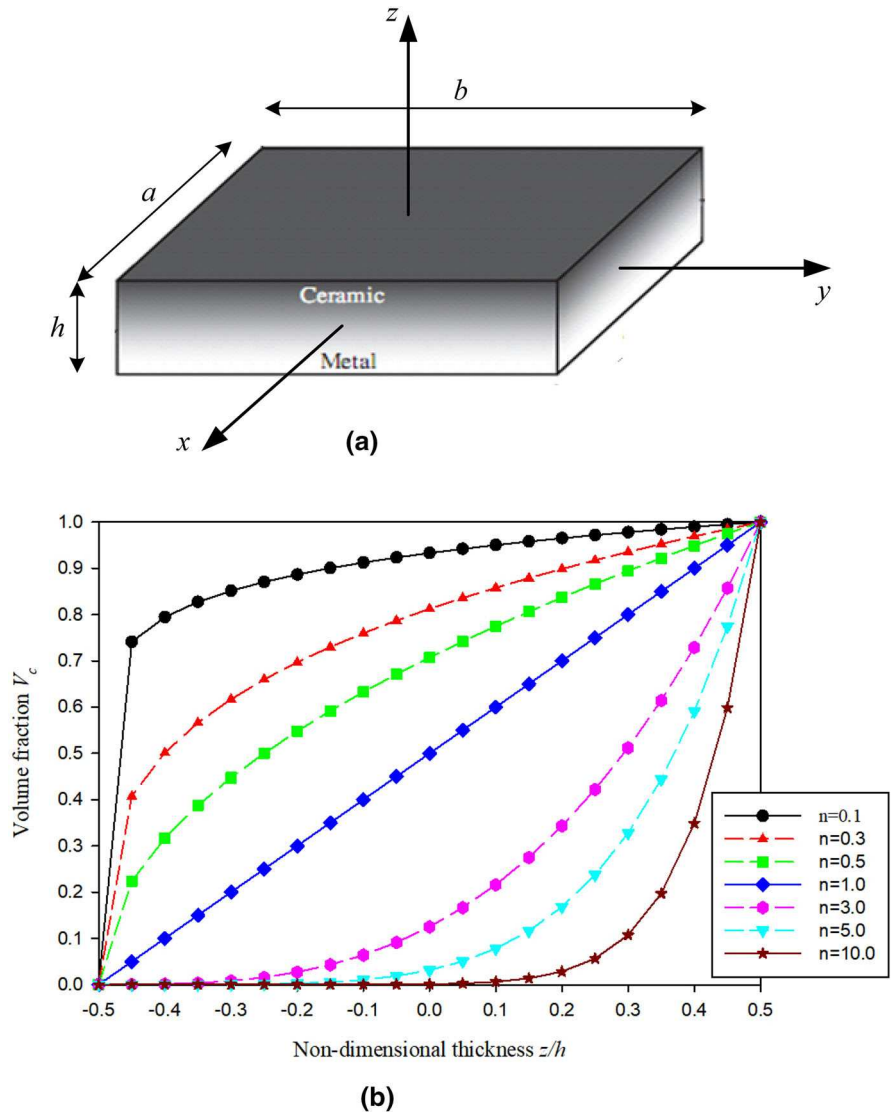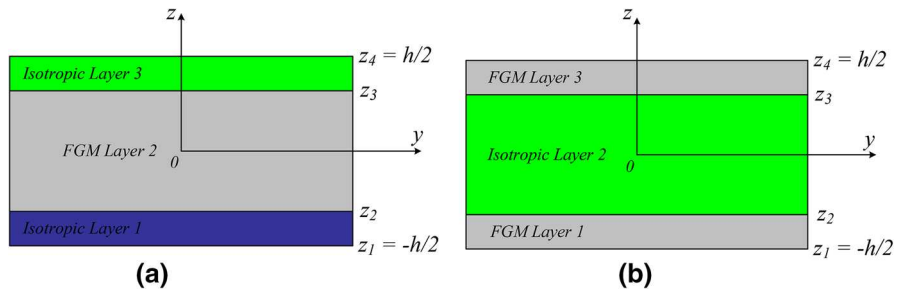
(a)

(b)

Fig. 2 The sandwich FGM plate: **a** FGM core and isotropic face sheets; **b** isotropic core and FGM face sheets

(a)

(b)

2.2 Formulation of new refined sin hyperbolic shear deformation plate theory

Let Ω be the domain occupied by the mid-plane of the FGM plate in $\mathbb{R}^2$. According to the conventional higher-order shear deformation theory (HSDT), its displacement field can be expressed in terms of five unknown variables as follows,

$$u(x,y,z) = u_0(x,y) + z\theta_x(x,y) + g(z)\left[\theta_x(x,y) + \frac{\partial w_0(x,y)}{\partial x}\right]$$

$$v(x,y,z) = v_0(x,y) + z\theta_y(x,y) + g(z)\left[\theta_y(x,y) + \frac{\partial w_0(x,y)}{\partial y}\right]$$

$$w(x,y,z) = w_0(x,y)$$

$$(4\text{a}, \text{b}, \text{c})$$

where u, v and w are the x-, y- and z-components of the displacement vector u of certain point (x,y,z) in the plate, respectively; $u_0(x,y)$, $v_0(x,y)$, and $w_0(x,y)$ are, respectively the x-, y- and z-components of the corresponding point $(x,y,0)$ on the plate mid-plane; $\theta_x(x,y)$ and $\theta_y(x,y)$ are the rotation angles of a transverse normal about the y- and x-axes; $g(z)$ represents shape function defining the distribution of the transverse shear strains and stresses across the plate thickness.

To derive the new refined sin hyperbolic shear deformation plate theory (N-RSHSDT), we use the assumptions of the four-variable refined plate theory (RPT) as follows: (1) the transverse displacement $u_0(x,y)$ is divided into bending $w_b(x,y)$ and shear $w_s(x,y)$ components, i.e., $w_0(x,y) = w_b(x,y) + w_s(x,y)$; (2) the rotations in the higher-order plate theory is expressed in terms of the bending component only $\theta_x = -\partial w_b(x,y)/\partial x$, $\theta_y = -\partial w_b(x,y)/\partial y$. In this regard, Eq. (4) can be rewritten as follows,

$$u(x,y,z) = u_0(x,y) - z\frac{\partial w_b(x,y)}{\partial x} + g(z)\frac{\partial w_s(x,y)}{\partial x}$$

$$v(x,y,z) = v_0(x,y) - z\frac{\partial w_b(x,y)}{\partial y} + g(z)\frac{\partial w_s(x,y)}{\partial y}$$

$$w(x,y,z) = w_b(x,y) + w_s(x,y)$$

$$(5\text{a}, \text{b}, \text{c})$$

Here we introduce a new sin hyperpolic function. From Eq. (5), it is clear that the displacement fields contain only four unknows, $u_0(x,y)$, $v_0(x,y)$, $w_b(x,y)$, $w_s(x,y)$, this leads to reduce the element stiffness, mass and geometric matrices, hence the computational time of the RPT is less than that of HSDT. In addition, the transverse shear strains shape function is chosen as $g(z) = f(z) - z$ such that the tangential value of the effective function $f(z) = h\sinh(z/h) - 4\cosh(1/2)z^3/3h^2$ at $z = \pm h/1$ are equal to zeros, satisfying the boundary conditions $\gamma_{xz} = \gamma_{yz} = 0$ on the top and bottom surfaces. Assuming that Lagrangian strains are infinitesimally small, the kinematic relations of strain–displacement can be expressed as follow,

$$\begin{Bmatrix} \varepsilon_x \\ \varepsilon_y \\ \gamma_{xy} \\ \gamma_{xz} \\ \gamma_{yz} \end{Bmatrix} = \begin{Bmatrix} \frac{\partial u_0(x,y)}{\partial x} - z\frac{\partial^2 w_b(x,y)}{\partial x^2} + g(z)\frac{\partial^2 w_s(x,y)}{\partial x^2} \\ \frac{\partial v_0(x,y)}{\partial x} - z\frac{\partial^2 w_b(x,y)}{\partial y^2} + g(z)\frac{\partial^2 w_s(x,y)}{\partial y^2} \\ \frac{\partial u_0(x,y)}{\partial y} + \frac{\partial v_0(x,y)}{\partial x} - 2z\frac{\partial^2 w_b(x,y)}{\partial x \partial y} + 2g(z)\frac{\partial^2 w_s(x,y)}{\partial x \partial y} \\ f'(z)\frac{\partial w_s(x,y)}{\partial x} \\ f'(z)\frac{\partial w_s(x,y)}{\partial y} \end{Bmatrix}$$

$$(6)$$

or in matrix form

$$\varepsilon = \begin{Bmatrix} \varepsilon_0 \\ 0 \end{Bmatrix} + \begin{Bmatrix} z\kappa^b + g(z)\kappa^s \\ f'(z)\gamma \end{Bmatrix} \qquad (7)$$

with

$$\varepsilon_0 = \begin{Bmatrix} \frac{\partial u_0(x,y)}{\partial x} \\ \frac{\partial v_0(x,y)}{\partial y} \\ \frac{\partial u_0(x,y)}{\partial y} + \frac{\partial v_0(x,y)}{\partial x} \end{Bmatrix}, \quad \kappa^b = \begin{Bmatrix} -\frac{\partial^2 w_b(x,y)}{\partial x^2} \\ -\frac{\partial^2 w_b(x,y)}{\partial y^2} \\ -2\frac{\partial^2 w_b(x,y)}{\partial x \partial y} \end{Bmatrix}$$

$$\kappa^s = \begin{Bmatrix} \frac{\partial^2 w_s(x,y)}{\partial x^2} \\ \frac{\partial^2 w_s(x,y)}{\partial y^2} \\ 2\frac{\partial^2 w_s(x,y)}{\partial x \partial y} \end{Bmatrix}, \quad \gamma = \begin{Bmatrix} \frac{\partial w_s(x,y)}{\partial x} \\ \frac{\partial w_s(x,y)}{\partial y} \end{Bmatrix}$$

$$(8\text{a}, \text{b}, \text{c}, \text{d})$$

It is worth noting that the present plate model is consistent as it does not require any shear correction factor, accounting for the sin hyperbolic distribution through the thickness of transverse shear strain, and satisfying the shear stress free surface conditions.

3 Meshless formulation for bending, free vibration and buckling of FGM plates

3.1 Moving Kriging shape function

In this subsection, the Moving Kriging shape function with their derivatives are briefly reviewed. A more detailed discussion for MKI method can be found in Bui et al. (2009). According to this method, an interpolation function $u^h(x)$ can be constructed by employing a known vector function $u(x_i)$ in a sub-domain Ω_x so that $\Omega_x \subseteq \Omega$. The sub-domain Ω_x which is also known as the influence or support domain. In this regard, the approximate function $u^h(x)$ can be expressed as follows,

$$\mathbf{u}^h(\mathbf{x}) = \left[\mathbf{p}^T(\mathbf{x})\mathbf{A} + \mathbf{r}^T(\mathbf{x})\mathbf{B}\right]\mathbf{u}(\mathbf{x}) \text{ or } \mathbf{u}^h(\mathbf{x}) = \sum_{I=1}^{n} \phi_I(x)\mathbf{u}_I \tag{9}$$

where $\phi_I(x)$ are shape functions, which are known to possesses the delta function property defined as,

$$\phi_I(\mathbf{x}) = \sum_{j=1}^{m} p_j(\mathbf{x})A_{jI} + \sum_{k=1}^{n} r_k(\mathbf{x})B_{kI} \tag{10}$$

wherein matrices A and B are calculated by

$$\mathbf{A} = \left(\mathbf{P}^T\mathbf{R}^{-1}\mathbf{P}\right)^{-1}\mathbf{P}^T\mathbf{R}^{-1}, \ \mathbf{B} = \mathbf{R}^{-1}(\mathbf{I} - \mathbf{PA}) \tag{11}$$

with I is the unit matrix, and p(x) in Eq. (9) denotes a vector of m basis functions, i.e.

$$\mathbf{p}^T(x) = [p_1(\mathbf{x}), p_2(\mathbf{x}), p_3(\mathbf{x})....,p_m(\mathbf{x})] \tag{12}$$

One should be noticed that n and m defined in this section are different from the gradient indices used in Sect. 2. Matrix $P(n \times m)$ consists of the values of the monomial basis functions at the nodal points

$$\mathbf{P} = \begin{bmatrix} p_1(\mathbf{x}_1) & p_2(\mathbf{x}_1) & \cdots & p_m(\mathbf{x}_1) \\ p_1(\mathbf{x}_2) & p_2(\mathbf{x}_2) & \cdots & p_m(\mathbf{x}_2) \\ \vdots & \vdots & \ddots & \vdots \\ p_1(\mathbf{x}_m) & p_2(\mathbf{x}_m) & \cdots & p_m(\mathbf{x}_m) \end{bmatrix} \tag{13}$$

and the vector r(x) in Eq. (9) has a formulation as follow,

$$\mathbf{r}^T(x) = [R(\mathbf{x}_1, \mathbf{x}), R(\mathbf{x}_2, \mathbf{x}),....R(\mathbf{x}_n, \mathbf{x})] \tag{14}$$

wherein $R(\mathbf{x}_i, \mathbf{x}_j)$ denotes the correlation function between pairs of the nodes x_i and x_j, and is the covariance of the value $u(x)$: $R(\mathbf{x}_i, \mathbf{x}_j) = \text{cov}[u(\mathbf{x}_i), u(\mathbf{x}_j)]$ and $R(\mathbf{x}_i, \mathbf{x}) = \text{cov}[u(\mathbf{x}_i), u(\mathbf{x})]$.

In the traditional MKI method (Chen et al. 2017; Bui et al. 2016), the Gaussian function with correlation parameter $\theta > 0$ is widely used as the correlation function having following formulation,

$$R(\mathbf{x}_i, \mathbf{x}_j) = e^{-\theta r_{ij}^2} \tag{15}$$

where $r_{ij} = \|\mathbf{x}_i - \mathbf{x}_j\|$. However, it is known that the quality of MK shape functions depend heavily on the correlation parameter θ (Bui et al. 2011; Bui and Nguyen 2011) which often causes the instability in the numerical model and its optimal value is still questionable. To overcome this drawback, we present new multi-quadric correlation functions, which depends only on the distance between the source point and the target point. It leads to the MKI shape function is stable and insensitive to the mesh node as follows,

$$R(\mathbf{x}_i, \mathbf{x}_j) = \sqrt{\left(\frac{1}{2l_c^2}\right)^2 + r_{ij}^2} \tag{16}$$

where l_c is the internal length factor of the model, which can be taken as the average distance between nodes in the model. The correlation matrix $R\left[R(\mathbf{x}_i, \mathbf{x}_j)\right]_{n \times n}$ is given by

$$\mathbf{R}\left[R(x_i, x_j)\right] = \begin{bmatrix} 1 & R(\mathbf{x}_1, \mathbf{x}_2) & \cdots & R(\mathbf{x}_1, \mathbf{x}_n) \\ R(\mathbf{x}_2, \mathbf{x}_1) & 1 & \cdots & R(\mathbf{x}_2, \mathbf{x}_n) \\ \vdots & \vdots & \ddots & \vdots \\ R(\mathbf{x}_n, \mathbf{x}_1) & R(\mathbf{x}_n, \mathbf{x}_2) & \cdots & 1 \end{bmatrix} \tag{17}$$

For the weak-form governing equation of the present plate model, not only the first-order derivatives, but also the second-order derivatives of the shape functions are required. Based on the MKI method, these derivatives are obtained by direct differentiation of Eq. (10), thus have the following formulations:

$$\phi_{I,i}(\mathbf{x}) = \sum_{j}^{m} p_{j,i}(\mathbf{x})A_{jI} + \sum_{k}^{n} r_{k,i}(\mathbf{x})B_{kI}$$

$$\phi_{I,ii}(\mathbf{x}) = \sum_{j}^{m} p_{j,ii}(\mathbf{x})A_{jI} + \sum_{k}^{n} r_{k,ii}(\mathbf{x})B_{kI} \tag{18a, b}$$

In conventional mesh-free approaches, scattered nodes which are used for interpolation and usually gathered by a circle or sphere defined by a radius and centred at the point of interest. In the present work, circle influence domains are employed for determining the nodes for the interpolation process. The radius size of the influence domain is defined by

$$d_m = \alpha d_c \qquad (19)$$

wherein d_c denotes as the characteristic length relative to the nodal spacing in the vicinity of the point of interest, and a scaling factor $\alpha > 1$ is used to control the size of influence domain.

3.2 Discrete governing equations

According to traditional meshfree method, the displacement filed in the middle FGM plate surface of present refine theory are approximated by Eq. (9) and expressed in term of vector form as follows,

$$\mathbf{u}^h = \begin{bmatrix} u^h & v^h & w_b^h & w_s^h \end{bmatrix}^T \text{ and } \mathbf{u}_I$$
$$= \begin{bmatrix} u_I & v_I & w_{bI} & w_{sI} \end{bmatrix}^T \qquad (20)$$

By substituting Eq. (9) into Eq. (8), one can obtain the following expressions after some mathematical manipulations:

$$\boldsymbol{\varepsilon}_0 = \sum_{I=1}^{n} \mathbf{B}_I^m \mathbf{u}_I, \ \boldsymbol{\kappa}^b = \sum_{I=1}^{n} \mathbf{B}_I^{b1} \mathbf{u}_I, \ \boldsymbol{\kappa}^s = \sum_{I=1}^{n} \mathbf{B}_I^{b2} \mathbf{u}_I, \ \boldsymbol{\gamma}$$
$$= \sum_{I=1}^{n} \mathbf{B}_I^s \mathbf{u}_I$$

$$(21)$$

wherein

$$\mathbf{B}_I^m = \begin{bmatrix} \phi_{I,x} & 0 & 0 & 0 \\ 0 & \phi_{I,y} & 0 & 0 \\ \phi_{I,y} & \phi_{I,x} & 0 & 0 \end{bmatrix}, \ \mathbf{B}_I^{b1} = \begin{bmatrix} 0 & 0 & -\phi_{I,xx} & 0 \\ 0 & 0 & -\phi_{I,yy} & 0 \\ 0 & 0 & -2\phi_{I,xy} & 0 \end{bmatrix}$$

$$\mathbf{B}_I^{b2} = \begin{bmatrix} 0 & 0 & 0 & \phi_{I,xx} \\ 0 & 0 & 0 & \phi_{I,yy} \\ 0 & 0 & 0 & 2\phi_{I,xy} \end{bmatrix}, \ \mathbf{B}_I^s = \begin{bmatrix} 0 & 0 & 0 & \phi_{I,x} \\ 0 & 0 & 0 & \phi_{I,y} \end{bmatrix}$$

$$(22a, b, c, d)$$

For the static bending problem of the FGM plate, the weak form can be stated as follows:

$$\int_{\Omega} \delta\boldsymbol{\varepsilon}^T \mathbf{D}^{\varepsilon} \boldsymbol{\varepsilon} d\Omega + \int_{\Omega} \delta\boldsymbol{\gamma}^T \mathbf{D}^s \boldsymbol{\gamma} d\Omega = \int_{\Omega} \delta(w_b + w_s)q_0 d\Omega$$

$$(23)$$

where q_0 is the transverse loading per unit area and

$$\boldsymbol{\varepsilon} = \begin{Bmatrix} \boldsymbol{\varepsilon}_0 \\ \boldsymbol{\kappa}^b \\ \boldsymbol{\kappa}^s \end{Bmatrix}, \quad \mathbf{D}^{\varepsilon} = \begin{bmatrix} A & B & E \\ B & C & K^{\varepsilon} \\ E & K^{\varepsilon} & H \end{bmatrix},$$

$$\mathbf{D}^s = \int_{-h/2}^{h/2} \mathbf{D}_s(z)dz$$

$$(24)$$

where the sub matrices are defined as

$$A_{ij}, B_{ij}, C_{ij}, E_{ij}, K_{ij}^{\varepsilon}, H_{ij}$$
$$= \int_{-h/2}^{h/2} \left[1, z, z^2, g(z), zg(z), g^2(z)\right] Q_{ij}dz \ D_{ij}^s$$
$$= \int_{-h/2}^{h/2} [f'(z)]^2 G_{ij}dz$$

$$(25a, b)$$

with the material matrices can be calculated by

$$Q = \frac{E(z)}{1 - v^2} \begin{bmatrix} 1 & v & 0 \\ v & 1 & 0 \\ 0 & 0 & (1-v)/2 \end{bmatrix}$$
$$G = \frac{E(z)}{2(1 + v)} \begin{bmatrix} 1 & 0 \\ 0 & 1 \end{bmatrix}$$

$$(26a, b)$$

For the free vibration problem of the FGM plate, the Hamilton's principle can be expressed as:

$$\int_{\Omega} \delta\boldsymbol{\varepsilon}^T \mathbf{D}^{\varepsilon} \boldsymbol{\varepsilon} d\Omega + \int_{\Omega} \delta\boldsymbol{\gamma}^T \mathbf{D}^s \boldsymbol{\gamma} d\Omega = \int_{\Omega} \delta\mathbf{u}^T \mathbf{m}\ddot{\mathbf{u}}d\Omega \quad (27)$$

where

$$\mathbf{m} = \begin{bmatrix} I_0 & I_1 & I_3 \\ I_1 & I_2 & I_4 \\ I_3 & I_4 & I_5 \end{bmatrix}, \ (I_0, I_1, I_2, I_3, I_4, I_5)$$
$$= \int_{-h/2}^{h/2} \rho(z) \left[1, z, z^2, g(z), zg(z), g^2(z)\right] dz \quad (28a, b)$$

With

$$\mathbf{u} = \left\{ \begin{array}{c} \mathbf{u}_0 \\ \mathbf{u}_b \\ \mathbf{u}_s \end{array} \right\}, \quad \mathbf{u}_0 = \left\{ \begin{array}{c} u^h \\ v^h \\ w_b^h + w_s^h \end{array} \right\} = \sum_{I=1}^{n} \mathbf{N}_I^1 \mathbf{u}_I$$

$$\mathbf{u}_b = \left\{ \begin{array}{c} -\partial w_b^h/\partial x \\ -\partial w_b^h/\partial y \\ 0 \end{array} \right\} = \sum_{I=1}^{n} \mathbf{N}_I^2 \mathbf{u}_I,$$

$$\mathbf{u}_s = \left\{ \begin{array}{c} \partial w_s^h/\partial x \\ \partial w_s^h/\partial y \\ 0 \end{array} \right\} = \sum_{I=1}^{n} \mathbf{N}_I^3 \mathbf{u}_I$$

$$(29a, b, c, d)$$

and

$$\mathbf{N}_I^1 = \begin{bmatrix} \phi_I & 0 & 0 & 0 \\ 0 & \phi_I & 0 & 0 \\ 0 & 0 & \phi_I & \phi_I \end{bmatrix}$$

$$\mathbf{N}_I^2 = \begin{bmatrix} 0 & 0 & -\phi_{I,x} & 0 \\ 0 & 0 & -\phi_{I,y} & 0 \\ 0 & 0 & 0 & 0 \end{bmatrix} \quad (30a, b, c)$$

$$\mathbf{N}_I^3 = \begin{bmatrix} 0 & 0 & 0 & \phi_{I,x} \\ 0 & 0 & 0 & \phi_{I,y} \\ 0 & 0 & 0 & 0 \end{bmatrix}$$

Finally, the weak form for the buckling analysis can be expressed as follows:

$$\int_\Omega \delta\boldsymbol{\varepsilon}^T \mathbf{D}^\varepsilon \boldsymbol{\varepsilon} d\Omega + \int_\Omega \delta\boldsymbol{\gamma}^T \mathbf{D}^s \boldsymbol{\gamma} d\Omega$$
$$+ \int_\Omega \nabla^T \delta(w_b + w_s) \hat{\sigma}_0 \nabla(w_b + w_s) d\Omega = 0 \qquad (31)$$

where $\nabla^T = [\partial/\partial x \quad \partial/\partial y]^T$ is the gradient operator and $\hat{\sigma}_0 = \begin{bmatrix} \sigma_x^0 & \tau_{xy}^0 \\ \tau_{xy}^0 & \sigma_y^0 \end{bmatrix}$ is the pre-stresses in-plane. By substituting Eq. (21) into Eqs. (23), (27) and (31) the discretized formulations of the static bending, free vibration and buckling analysis of the FGM plate can be rewritten as following:

$$\mathbf{Ku} = \mathbf{F}, \quad (\mathbf{K} - \omega^2 \mathbf{M})\mathbf{u} = \mathbf{0}, \quad (\mathbf{K} - \omega^2 \mathbf{K}_g)\mathbf{u} = \mathbf{0} \qquad (32a, b, c)$$

where the stiffness matrix K is calculated by

Table 1 Material properties of the FG plates used for the analysis

Property	Aluminium (Al)	Ceramic		
		Alumina (Al$_2$O$_3$)	Zirconia-1 (ZrO$_2$-1)	Zirconia-2 (ZrO$_2$-2)
E (GPa)	70	380	200	151
υ	0.3	0.3	0.3	0.3
ρ (kg/m^3)	2707	3800	5700	3000

Table 2 Normalized displacement $\bar{w}$ of a simply supported square plate using different meshes and scaling factors

Mesh	Scaling factor α							
	2.0	2.1	2.2	2.3	2.4	2.5	3.0	3.5
17×17	0.4431	0.6576	0.6603	0.6643	0.6656	0.6705	0.6731	0.7131
21×21	0.4767	0.6506	0.6509	0.6546	0.6553	0.6557	0.6755	0.7220
25×25	0.2757	0.6455	0.6460	0.6485	0.6486	0.6511	0.6607	0.7125
29×29	0.6100	0.6425	0.6427	0.6445	0.6446	0.6465	0.6551	0.6949
33×33	0.6142	0.6404	0.6406	0.6420	0.6421	0.6432	0.6499	0.6887
CLT (Carrera and Brischetto 2008)	0.6070							
FSDT (Carrera and Brischetto 2008)	0.6337							
CUF (Carrera et al. 2011)	0.6337							
HSDT (Neves et al. 2013)	0.6350							

$$\mathbf{K} = \int_\Omega \left\{ \begin{matrix} \mathbf{B}_I^m \\ \mathbf{B}_I^{b1} \\ \mathbf{B}_I^{b2} \end{matrix} \right\}^T \begin{bmatrix} A & B & E \\ B & C & K^\varepsilon \\ E & K^\varepsilon & H \end{bmatrix} \left\{ \begin{matrix} \mathbf{B}_I^m \\ \mathbf{B}_I^{b1} \\ \mathbf{B}_I^{b2} \end{matrix} \right\} d\Omega$$
$$+ \int_\Omega (\mathbf{B}^s)^T \mathbf{D}^s \mathbf{B}^s d\Omega \qquad (33)$$

The load vector F is computed as follows:

$$F = \int_\Omega q_0 N d\Omega \text{ where } N_I = \begin{bmatrix} 0 & 0 & \phi_I & \phi_I \end{bmatrix}^T \quad (34)$$

The mass matrix M is expressed as:

$$\mathbf{M} = \int_\Omega \left\{ \begin{matrix} \mathbf{N}^1 \\ \mathbf{N}^2 \\ \mathbf{N}^3 \end{matrix} \right\}^T \begin{bmatrix} I_0 & I_1 & I_3 \\ I_1 & I_2 & I_4 \\ I_3 & I_4 & I_5 \end{bmatrix} \left\{ \begin{matrix} \mathbf{N}^1 \\ \mathbf{N}^2 \\ \mathbf{N}^3 \end{matrix} \right\} d\Omega \qquad (35)$$

The geometric stiffness matrix K_g is obtained by

$$K_g = \int_\Omega (B^g)^T \hat{\sigma}_0 B^g d\Omega \text{ where } B_I^g$$
$$= \begin{bmatrix} 0 & 0 & \phi_{I,x} & \phi_{I,x} \\ 0 & 0 & \phi_{I,y} & \phi_{I,y} \end{bmatrix} \qquad (36a, b)$$

From Eq. (22), it is observed that two matrices $\mathbf{B}_I^{b1}$ and $\mathbf{B}_I^{b2}$ consist of the second-order derivatives of the MKI shape function, hence the approximate displacements must have to the C^1-connuity. As a result, a second-order polynomial basis given in Eq. (12) is used to establish the shape functions as follow,

$$p^T(x) = \begin{Bmatrix} 1 & x & y & x^2 & xy & y^2 \end{Bmatrix} \qquad (37)$$

In this regard, a quadratic polynomial form of basic functions $(m = 6)$ is employed to construct MKI shape function, and a background mesh with 4×4 Gauss points are also used.

Table 3 Normalized deflection of an Al/ZrO$_2$-1 square plate with different length-thickness ratio a/h and gradient indices n

Boundary condition	a/h	Method	$n = 0$	$n = 0.5$	$n = 1$	$n = 2$
SSSS	5	S-FSDT-MK (Vu et al. 2017)	0.1723	0.2331	0.2723	0.3116
		R-STSDT-MK (Vu et al. 2018)	0.1721	0.2325	0.2725	0.3142
		FSDT-kp-Ritz (Lee et al. 2009)	0.1722	0.2403	0.2811	0.3221
		Present	0.1773	0.2395	0.2806	0.3238
	100	S-FSDT-IGA (Carrera and Brischetto 2008)	0.1423	0.1949	0.2284	0.2597
		R-STSDT-MK (Vu et al. 2018)	0.1427	0.1954	0.2290	0.2603
		R-SSDT-MK (Vu et al. 2017)	0.1483	0.2031	0.2379	0.2705
		Present	0.1457	0.1996	0.2339	0.2659
SFSS	5	S-FSDT-IGA (Carrera and Brischetto 2008)	0.3164	0.4299	0.5032	0.5752
		R-STSDT-MK (Vu et al. 2018)	0.3153	0.4278	0.5013	0.5757
		Present	0.3233	0.4384	0.5138	0.5902
	100	S-FSDT-MK (Vu et al. 2017)	0.2777	0.3805	0.4458	0.5069
		R-STSDT-MK (Vu et al. 2018)	0.2766	0.3790	0.4440	0.5047
		Present	0.2816	0.3858	0.4519	0.5138
SFSF	5	S-FSDT-IGA (Carrera and Brischetto 2008)	0.5083	0.6918	0.8099	0.9247
		R-STSDT-MK (Vu et al. 2018)	0.5061	0.6879	0.8061	0.9239
		FSDT-kp-Ritz (Lee et al. 2009)	0.5061	0.7029	0.8214	0.9423
		Present	0.5162	0.7014	0.8219	0.9423
	100	S-FSDT-IGA (Carrera and Brischetto 2008)	0.4584	0.6281	0.7360	0.8367
		R-STSDT-MK (Vu et al. 2018)	0.4564	0.6252	0.7325	0.8327
		R-SSDT-MK (Vu et al. 2017)	0.4627	0.6339	0.7427	0.8443
		Present	0.4623	0.6333	0.7419	0.8434

4 Numerical results and discussions

In this section, several numerical examples are presented and discussed to verify the accuracy of the proposed approach in predicting the static bending, free vibration and buckling responses of isotropic and sandwich FG plates with square shape. For convenience, the boundaries of these plates are denoted as follows: completely free (F), simply supported (S) or fully clamped (C) edges. Both thin and thick plates are considered through the specified thickness-span aspect ratios.

4.1 Effect of the scaling factor on the solution accuracy

Consider a fully-simply supported sandwich square plate-type B with the length to thickness ratio $a/h = $

10 consisting of three layers. The bottom skin is aluminium with the thickness and young's modulus are $h_b = 0.1$ h and $E_m = 70$ GPa, respectively. The top skin is alumina with the thickness and young's modulus are $h_t = 0.1$ h and $E_c = 380$ GPa, respectively. Further data of plate is given in Table 1. The core skin is FGM with effective material properties defined by Eq. (1) and graded from aluminium to alumina with the gradient index $n = 1.0$. The plate is subjected to the bi-sinusoidal transverse mechanical load $q_0 = \bar{q}_0 \sin(\pi x/a) \sin(\pi y/b)$.

To investigate the influence of scaling factor α on the accuracy of numerical solution, the normalized displacement $\bar{w} = \frac{10E_c h^3}{q_0 a^4} w\left(\frac{a}{2}, \frac{b}{2}, 0\right)$ at the centre of plate is calculated using different sets of 17×17, 21×21, 25×25, 29×29 and 33×33 combined with different scaling factors. Results are presented
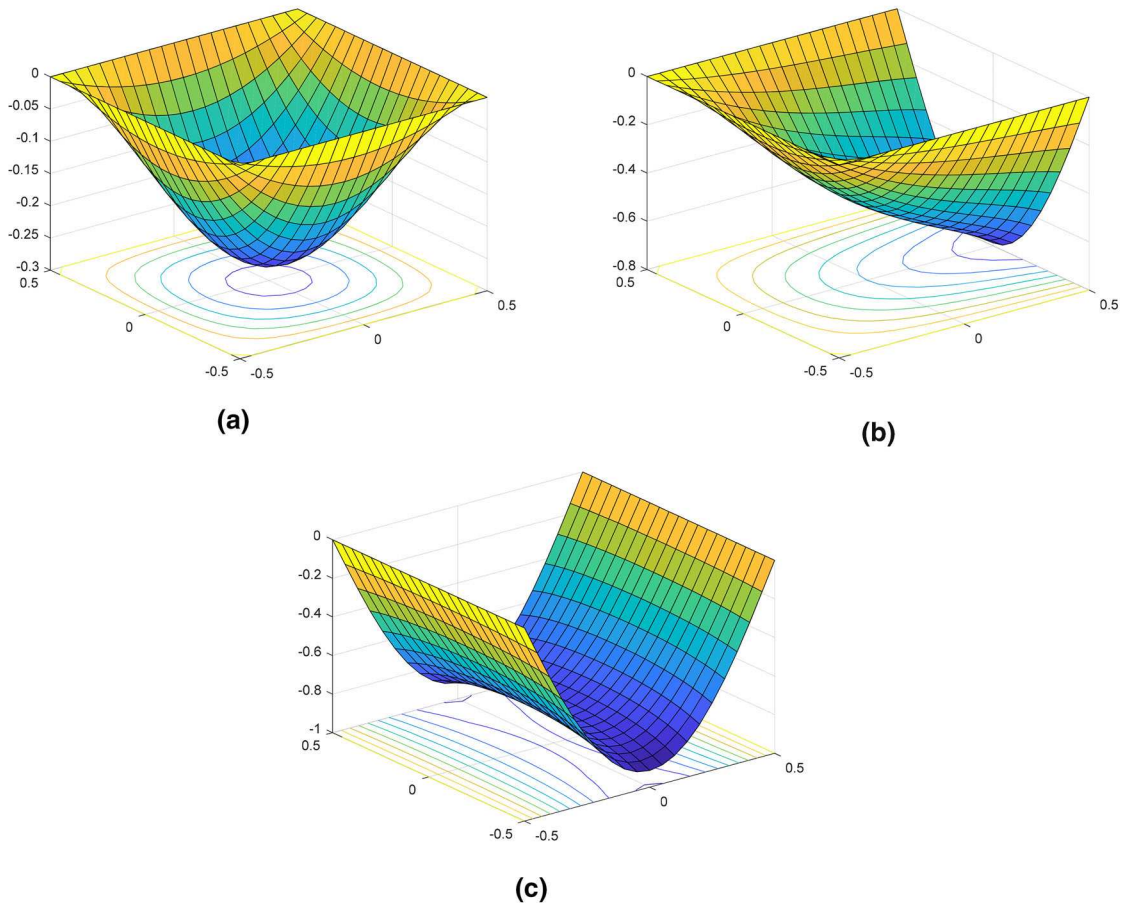

Fig. 3 Deformation shapes of the FGM plates (type A) with $n = 1$ and $a/h = 5$ different boundary conditions: **a** SSSS, **b** SFSS, **c** SFSF

and compared with those from the classical plate theory (CPT) (Carrera and Brischetto 2008), first-order shear deformation theory (FSDT) (Carrera and Brischetto 2008), higher-order shear deformation theory (HSDT) (Neves et al. 2013) and Carrera's Unified Formulation (CUF) (Carrera et al. 2011) in Table 2. As seen in the table, the multi-quadric function can yield the excellent convergence and ensure for the stable numerical computation when $2.0 < \alpha < 3.0$. We consider that a value of $\alpha = 2.1$ with the fine set of 21×21 can be employed in the following computation.

4.2 Static bending analysis

4.2.1 Isotropic FGM plates (type A)

In this example, an isotropic FGM square plate of type A subjected to a uniform load q_0 with various boundary conditions such as SSSS, SFSS, SFSF is considered. The plate is graded from aluminium at the bottom to zirconia-1 at the top of the plate. The material property of this plate is listed in Table 1. The central deflection also has the normalized form of $\bar{w} = \frac{100 w_c E_m h^3}{12(1-v_m^2)q_0 a^4}$. Table 3, we present the results obtained with the referenced theories using different values of the gradient indices and length to thickness ratios $a/h = 5, 100$. The deformation shapes of the plate with different boundary conditions are shown in Fig. 3. It can be concluded that numerical results obtained by the present method are agreed well with those obtained by reference methods such as RPT combined with the MKI methods (S-FSDT Vu et al. 2017; R-STSDT Vu et al. 2018; R-SSDT Vu et al. 2017) and FSDT-kp-Ritz (Lee et al. 2009) method.

It is worth nothing that the deflection magnitude increases when the boundary condition changes from

Table 4 Normalized deflection of a sandwich square plate-type C ($a/h = 10$)

Kind of sandwich plate-type C	Method	$n = 0.0$	$n = 0.5$	$n = 1.0$	$n = 2.0$	$n = 5.0$	$n = 10.0$
2–1–2	CLT (Neves et al. 2012)	0.1856	–	0.2942	0.3394	0.3779	0.3894
	FSDT (Neves et al. 2012)	0.1961	–	0.3075	0.3541	0.3942	0.4066
	HSDT (Bessaim et al. 2013)	0.1949	0.2614	0.3043	0.3500	0.3893	0.4015
	ZZF (Neves et al. 2012)	0.1961	0.2667	0.3090	0.3542	0.3930	0.4051
	Present	0.1970	0.2644	0.3078	0.3539	0.3935	0.4058
2–1–1	CLT (Neves et al. 2012)	–	–	–	–	–	–
	FSDT (Neves et al. 2012)	–	–	–	–	–	–
	HSDT (Bessaim et al. 2013)	0.1949	0.2560	0.2945	0.3350	0.3698	0.3811
	ZZF (Neves et al. 2012)	0.1961	0.2614	0.2995	0.3399	0.3746	0.3861
	Present	0.1970	0.2590	0.2982	0.3394	0.3748	0.3862
1–1–1	CLT (Neves et al. 2012)	0.1856	–	0.2803	0.3207	0.3587	0.3724
	FSDT (Neves et al. 2012)	0.1961	–	0.2930	0.3344	0.3736	0.3879
	HSDT(Bessaim et al. 2013)	0.1949	0.2530	0.2901	0.3307	0.3690	0.3830
	ZZF(Neves et al. 2012)	0.1961	0.2583	0.2949	0.3351	0.3729	0.3868
	Present	0.1970	0.2559	0.2934	0.3345	0.3731	0.3872
2–2–1	CLT (Neves et al. 2012)	0.1856	–	0.2692	0.3041	0.3369	0.3492
	FSDT (Neves et al. 2012)	0.1961	–	0.2817	0.3174	0.3512	0.3640
	HSDT (Bessaim et al. 2013)	0.1949	0.2466	0.2787	0.3136	0.3465	0.3589
	ZZF (Neves et al. 2012)	0.1961	0.2519	0.2838	0.3186	0.3514	0.3637
	Present	0.1970	0.2495	0.2822	0.3177	0.3512	0.3638
1–2–1	CLT (Neves et al. 2012)	0.1856	–	0.2596	0.2910	0.3228	0.3361
	FSDT (Neves et al. 2012)	0.1961	–	0.2717	0.3037	0.3363	0.3500
	HSDT (Bessaim et al. 2013)	0.1949	0.2407	0.2692	0.3006	0.3326	0.3459
	ZZF (Neves et al. 2012)	0.1961	0.2460	0.2740	0.3053	0.3370	0.3503
	Present	0.1970	0.2435	0.2723	0.3041	0.3364	0.3499

SSSS, SFSS to SFSF or the length to thickness ratio decreases from 100 to 5, since the structural stiffness is decreased. Conversely, the deflection magnitude decreases as the gradient index n reduces, because the property of plates approached closer to that of the ceramic constituent when the gradient index decreases, and consequently the stiffness of the resulting plates gradually increases.
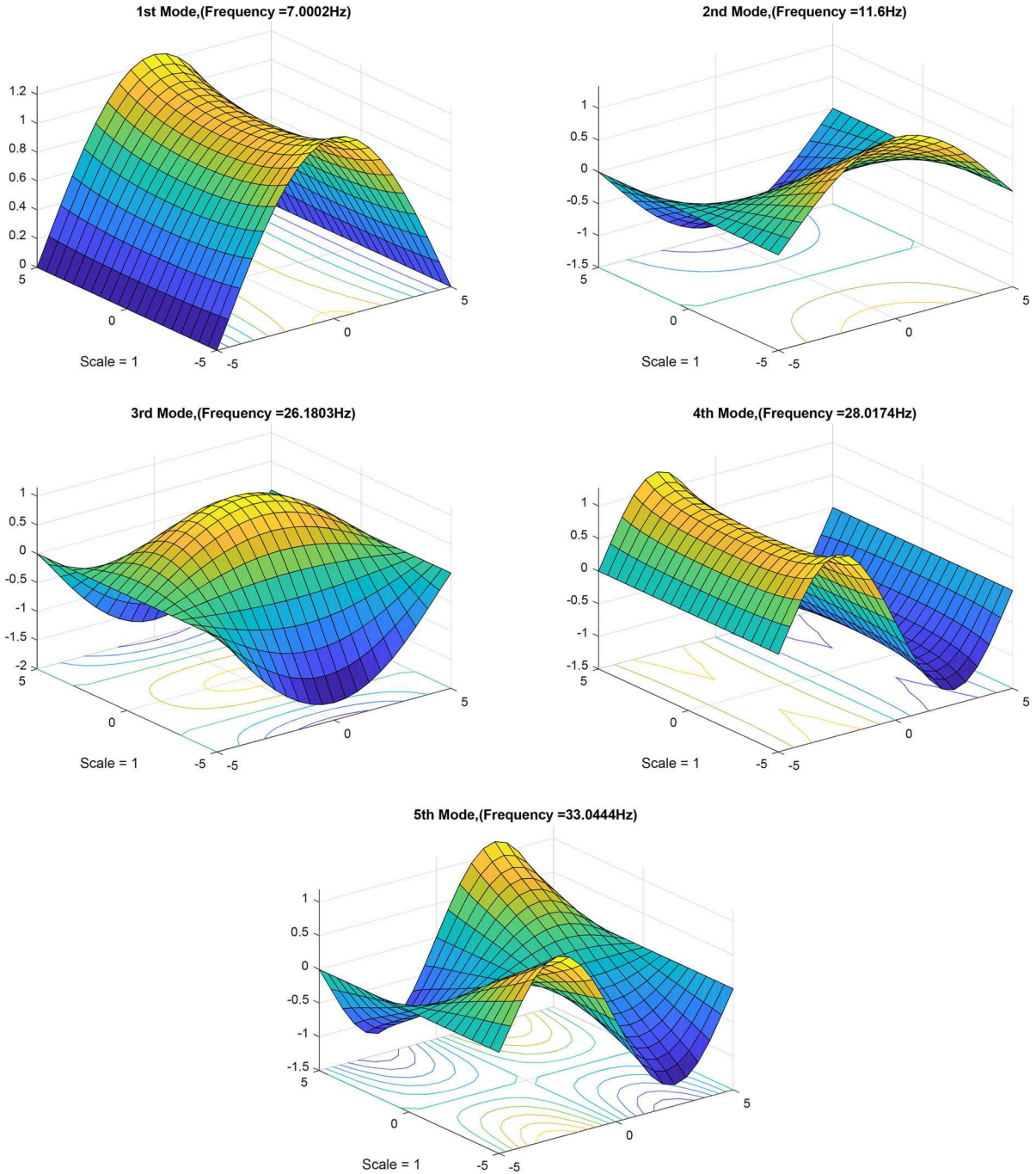

Fig. 4 First five mode shapes of the Al/Al$_2$O$_3$ freely—simply supported square plate

4.2.2 Sandwich plates with isotropic core and FGM face sheets (type C)

In this example, static bending of a simply supported sandwich FGM square plate-type C with material made from the aluminium and zirconia-2 is analyzed. The material parameters of this plate are provided in

Table 1. The core layer is independent with respect to values of the gradient index n, which is a fully ceramic layer. However, a value of n equal to zero represents a fully ceramic plate. The transverse displacement is presented in normalized as $\bar{w} = \frac{10E_o h}{\bar{q}_0 a^2} w\left(\frac{a}{2}, \frac{b}{2}, 0\right)$ and $q_0 = 1$, $E_0 = 1$ GPa. Table 4 shows the results obtained by the reference methods with considering

Table 5 The first five mode normalized natural frequencies of an Al/Al$_2$O$_3$ thin plate with various boundary conditions and gradient indices

n	Method	Mode 1	Mode 2	Mode 3	Mode 4	Mode 5
(a) SFSF						
1	CPT-neu based IGA (Yin et al. 2013)	43.1596	72.2984	164.5401	174.5012	209.4085
	S-FSDT-MK (Vu et al. 2018)	43.2374	71.2856	161.2857	175.8363	206.5470
	Exact (Baferani et al. 2011)	43.0872	72.2001	164.3911	–	–
	Present	42.9806	71.7756	162.0638	171.5960	204.8737
2	CPT-neu based IGA (Yin et al. 2013)	39.2395	65.7314	149.5922	158.6496	190.3849
	S-FSDT-MK (Vu et al. 2018)	39.3354	64.9015	146.9400	160.1133	188.3231
	Exact (Baferani et al. 2011)	39.1666	65.6400	149.0583	–	–
	Present	39.0828	65.2660	147.3546	156.0896	186.3556
(b) SSSS						
1	CPT-neu based IGA (Yin et al. 2013)	88.4501	221.1011	221.1011	353.7127	442.1697
	S-FSDT-MK (Vu et al. 2018)	88.4983	223.1878	223.1878	359.3324	448.5040
	Exact (Baferani et al. 2011)	88.3093	221.0643	–	353.6252	–
	Present	87.4004	215.2458	215.2458	337.5635	421.0957
2	CPT-neu based IGA (Yin et al. 2013)	80.4160	201.0155	201.0155	321.5761	401.9929
	S-FSDT-MK (Vu et al. 2018)	80.6550	204.0120	204.0120	330.2422	411.6235
	Exact (Baferani et al. 2011)	80.3517	200.8793	–	321.4069	–
	Present	79.4630	195.7338	195.7338	306.9145	383.1018
(c) SCSC						
1	CPT-neu based IGA (Yin et al. 2013)	129.7269	245.2758	310.6242	423.7400	457.9482
	S-FSDT-MK (Vu et al. 2018)	129.9227	246.0544	311.5795	429.6741	456.0445
	Exact (Baferani et al. 2011)	129.6496	245.1310	–	423.6904	–
	Present	129.2264	239.9096	305.1543	408.8027	438.4519
2	CPT-neu based IGA (Yin et al. 2013)	117.9435	222.9939	282.4052	385.2402	416.3375
	S-FSDT-MK (Vu et al. 2018)	117.9340	223.2098	279.5867	389.7883	412.6522
	Exact (Baferani et al. 2011)	117.8104	222.8111	–	385.0672	–
	Present	117.5411	218.2121	277.5496	371.8758	398.9104
(d) CCCC						
1	CPT-neu based IGA (Yin et al. 2013)	161.2484	328.8502	328.8502	484.8293	589.5860
	S-FSDT-MK (Vu et al. 2018)	161.0227	328.6780	328.6780	488.7393	591.5320
	Present	160.8461	322.9511	322.9511	467.6309	564.5060
2	CPT-neu based IGA (Yin et al. 2013)	146.6016	298.9753	298.9753	440.7781	536.0119
	S-FSDT-MK (Vu et al. 2018)	146.9611	297.6900	297.6900	441.7803	531.8659
	Present	146.3175	293.7530	293.7530	425.4270	513.5280

different values of gradient index and kind of the sandwich FGM and compared to our results. It is clear that present method correlates excellently with previous theories in the literature (Neves et al. 2012; Bessaim et al. 2013).

4.3 Free vibration analysis

4.3.1 Isotropic FGM plates (type A)

In this example we study the free vibration of an Al/ Al_2O_3 isotropic square thin plate with a length to
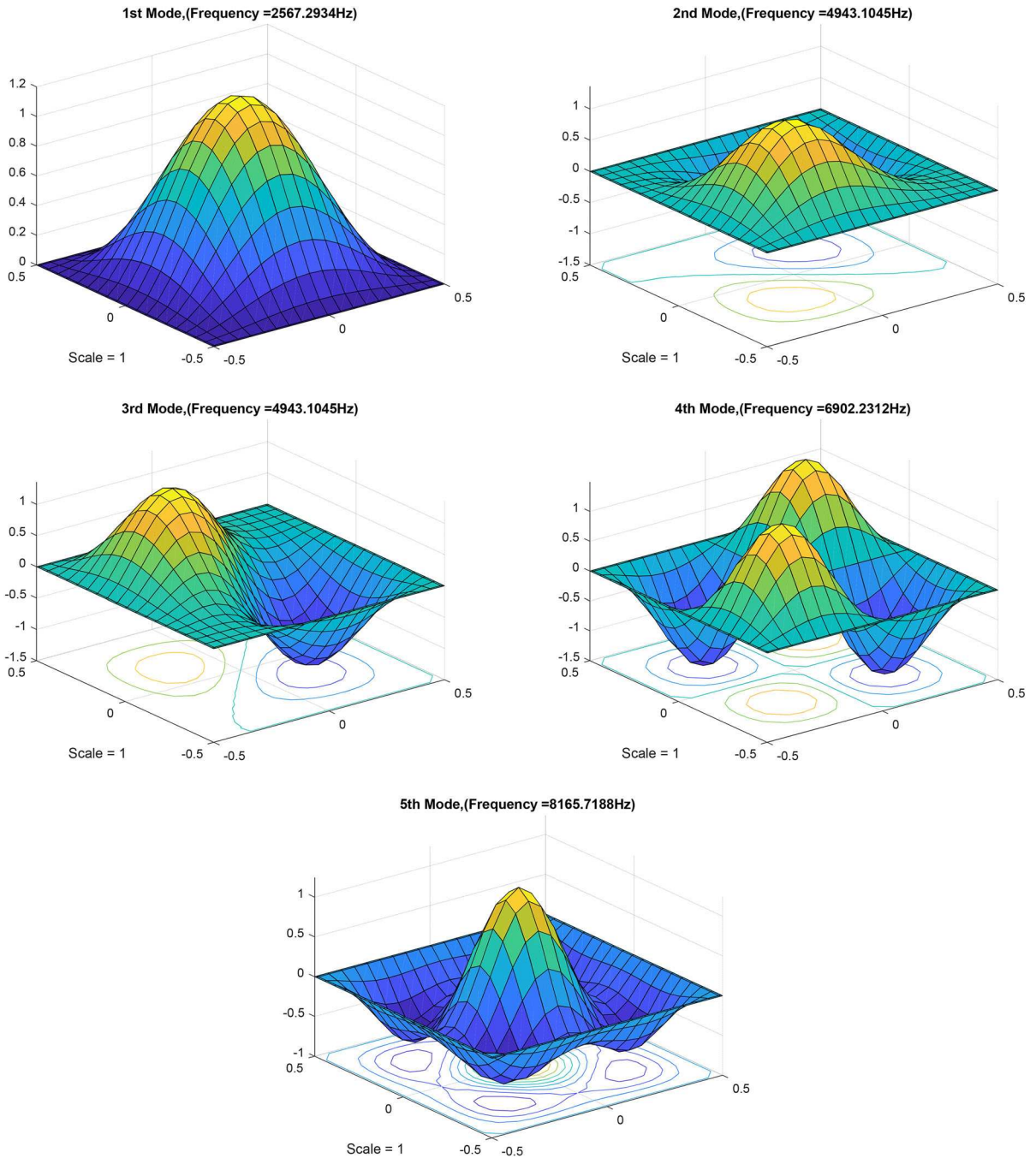

Fig. 5 First five mode shapes of the fully clamped square plate

Table 6 The first five mode normalized natural frequencies of square [1/8/1] of sandwich FGM plates of Type B with $n = 1$ and ($h/b = 0.01, 0.1$)

a/h	Method	Mode 1	Mode 2	Mode 3	Mode 4	Mode 5
(a) SSSS						
100	3D (Li et al. 2008)	1.5760	3.9379	3.9379	6.2972	7.8686
	Present	1.5649	3.9048	3.9048	6.2115	7.7989
10	3D (Li et al. 2008)	1.5221	3.6295	3.6295	5.5679	6.7829
	Present	1.5123	3.6037	3.6037	5.5046	6.7337
(b) CCCC						
100	3D (Li et al. 2008)	2.8830	5.8720	5.8720	8.6495	10.5180
	Present	2.7942	5.6682	5.6682	8.2370	10.1953
10	3D (Li et al. 2008)	2.6050	4.9630	4.9630	6.9516	8.1872
	Present	2.5673	4.9431	4.9431	6.9022	8.1657

Table 7 The first mode normalized natural frequencies of square with difference layer thickness ratios and gradient indices of sandwich FGM plates of Type C ($a/h = 10$)

n	Method	Type of sandwich plate					
		1–0–1	2–1–2	2–1–1	1–1–1	2–2–1	1–2–1
0.5	3D (Li et al. 2008)	1.4461	1.4861	1.5084	1.5213	1.5493	1.5766
	SSDT (Zenkour 2005)	1.4443	1.4842	1.5126	1.5193	1.5520	1.5745
	TSDT (Zenkour 2005)	1.4442	1.4842	1.5125	1.5192	1.5520	1.5745
	Present	1.4406	1.5027	1.5026	1.5153	1.5432	1.5704
1.0	3D (Li et al. 2008)	1.2447	1.3018	1.3351	1.3552	1.3976	1.4413
	SSDT (Zenkour 2005)	1.2433	1.3002	1.3489	1.3534	1.4079	1.4393
	TSDT (Zenkour 2005)	1.2432	1.3001	1.3489	1.3533	1.4079	1.4393
	Present	1.2402	1.2969	1.3301	1.3499	1.3921	1.4355
5.0	3D (Li et al. 2008)	0.9448	0.9810	1.0294	1.0453	1.1098	1.1757
	SSDT (Zenkour 2005)	0.9463	0.9820	1.0744	1.0448	1.1474	1.1740
	TSDT (Zenkour 2005)	0.9460	0.9818	1.0743	1.0447	1.1473	1.1740
	Present	0.9439	0.9796	1.0283	1.0421	1.1064	1.1709
10.0	3D (Li et al. 2008)	0.9273	0.9418	0.9893	0.9952	1.0610	1.1247
	SSDT (Zenkour 2005)	0.9288	0.9433	1.0455	0.9952	1.0415	1.1346
	TSDT (Zenkour 2005)	0.9284	0.9430	1.0386	0.9955	1.1053	1.1231
	Present	0.9265	0.9409	0.9900	0.9932	1.0587	1.1203

thickness ratio of $a/h = 100$ under different boundary conditions. Natural frequency has been non-dimensioned as follows: $\omega^* = \omega \pi^2 (a^2/h) \sqrt{\rho_m/E_m}$. Figure 4 plots first five mode shapes of the square thin plate with SFSF boundary conditions. In Table 5, we present the results obtained with proposed and available methods (Vu et al. 2018; Yin et al. 2013; Baferani et al. 2011) considering various values of gradient indices. It is concluded that the present refined plate theory predicts the natural frequencies with the same accuracy degree as that of exact method (Baferani et al. 2011). It is seen that the results decrease as the amount of gradient indices increase.

The effect of the boundary conditions on the natural frequency is observed from Table 5. It has been established that the natural frequencies of the plate with all edges clamped are higher than those of the plate with edges free and simply support. The normalized frequency magnitude increases when the boundary condition changes from SFSF, SSSS, SCSC to CCCC, due to the increase of the structural stiffness.

4.3.2 Sandwich plate with FGM core and isotropic face sheets (type B)

In this example we consider the normalized frequency of a sandwich square plate-type B with boundary type
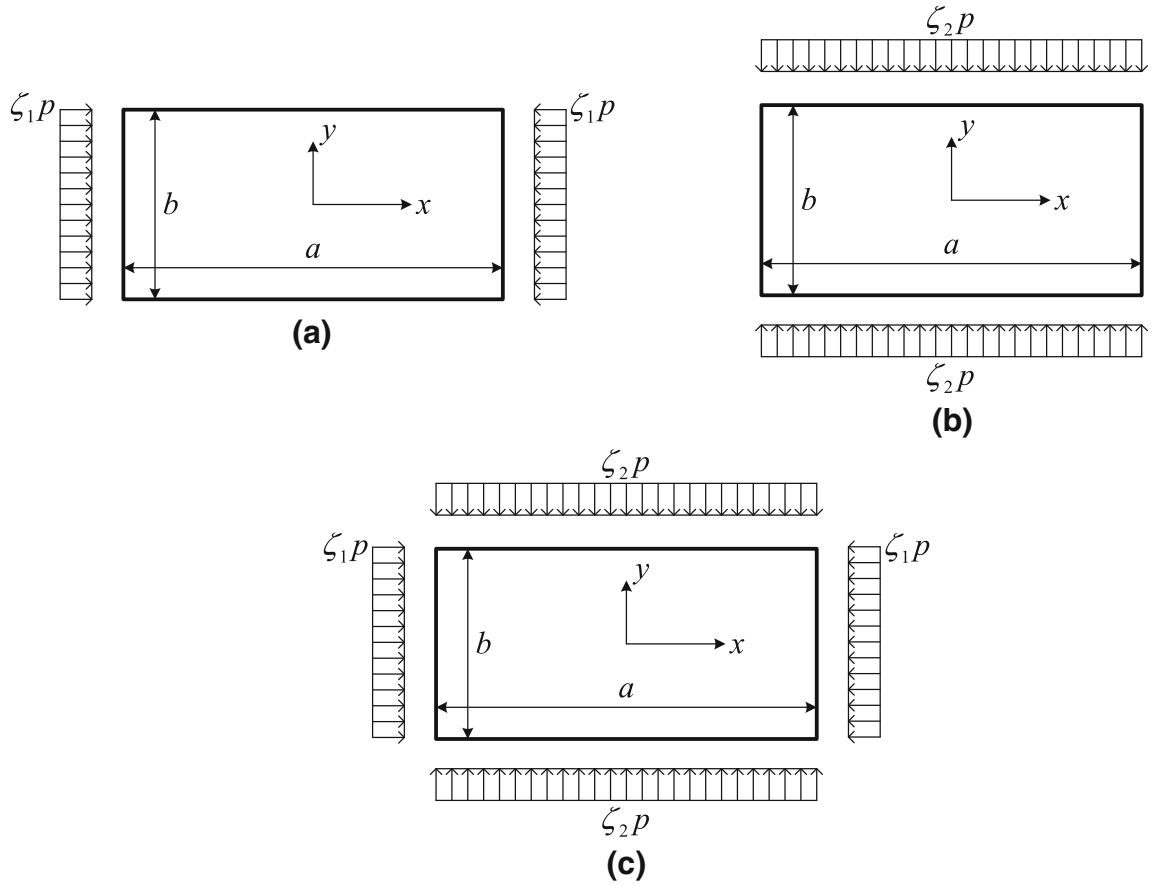
Fig. 6 A rectangular FG plate subjected to in-plane loads: **a** uni-axial compression along x-axis ($\zeta_1 = -1$, $\zeta_2 = 0$); **b** uni-axial compression along y-axis ($\zeta_1 = 0$, $\zeta_2 = -1$); **c** biaxial compression ($\zeta_1 = -1$, $\zeta_2 = -1$)

of SSSS and CCCC. The top and bottom face of FGM are alumina and aluminium, respectively. Its material properties are given in Table 1. The material distribution is chosen as $[1/8/1]$ with $n = 1$, while the normalized frequency is defined as $\omega^* = \omega\,(a^2/h)\sqrt{\rho_0/E_0}$ and $\rho_0 = 1\ \text{kg/m}^3$ and $E_0 = 1$ GPa. Figure 5 depicts the first five mode shapes of the square plate with edges fully clamped. Table 6 shows the results of the normalized frequency obtained by the present method comparing with those obtained by using Ritz method based on the 3D linear elasticity theory of Li et al. (2008). It is worth noting that a good agreement between the present and reference solution and as expected, the normalized frequency magnitude increase when the boundary condition changes from SSSS to CCCC.

4.3.3 Sandwich plates with isotropic core and FGM face sheets (type C)

In this example we investigate the normalized frequency of a SSSS sandwich square plate-type C. The plate consists of a pure ceramic core, FGM skins with metal-rich at top and bottom surfaces. The effective properties are calculated by the rule of mixture. Material properties of alumina and aluminium are given in Table 1. The normalized frequency is defined as $\omega^* = \omega\,(a^2/h)\sqrt{\rho_0/E_0}$ with $\rho_0 = 1\ \text{kg/m}^3$ and $E_0 = 1$ GPa. The results of the normalized frequency obtained with different methods accounted for various thickness ratios and gradient indices are gathered in Table 7. Very good agreement between reference methods (Li et al. 2008; Zenkour 2005) and the present method are obtained.
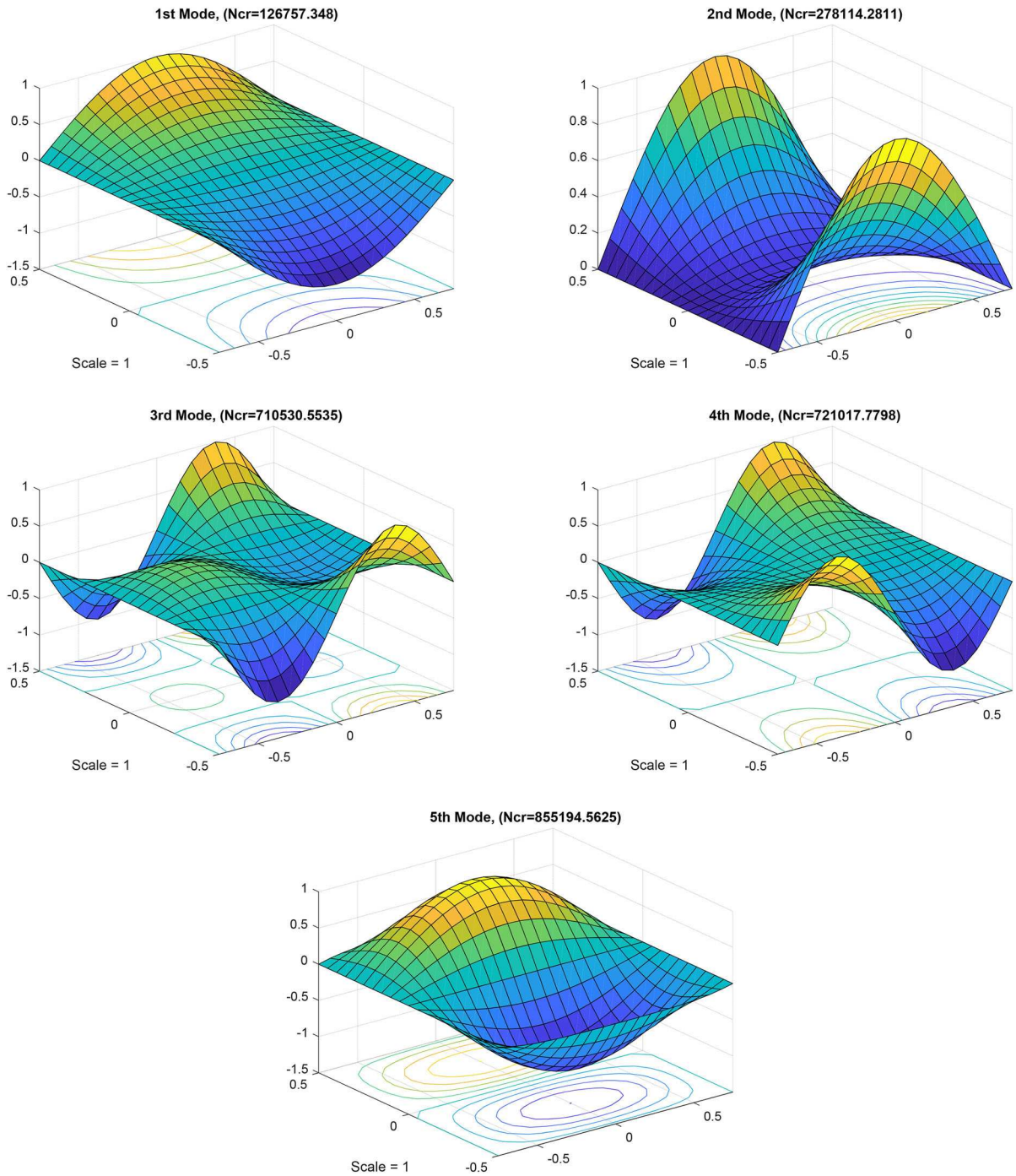
Fig. 7 First five buckling modes of the Al/Al$_2$O$_3$ free—simply supported square plate with $a/b = 1.5$, $(\zeta_1 = 0, \ \zeta_2 = -1)$

4.4 Buckling analysis

In this section, the buckling analysis of a rectangular FGM plate subjected to biaxial or uni-axial in-plane loading is considered. The problem geometry and loading are shown in Fig. 6. The pre-buckling forces are obtained by imposing the equilibrium requirements, as follows:

Table 8 Buckling loads (MN/m) for Al/Al$_2$O$_3$ rectangular plate with different boundary conditions and aspect ratios

n	Method	$a/b = 1.5$ (ζ_1, ζ_2)			$a/b = 1.0$ (ζ_1, ζ_2)		
		$-1, 0$	$0, -1$	$-1, -1$	$-1, 0$	$0, -1$	$-1, -1$
(a) SFSF							
1	S-FSDT based IGA (Yin et al. 2014)	0.0714	0.1305	0.0702	0.1630	0.3497	0.1596
	Levy (Mohammadi et al. 2010)	0.0714	0.1305	0.0702	0.1630	0.3497	0.1712
	R-STSDT-MK (Vu et al. 2018)	0.0716	0.1329	0.0705	0.1632	0.3535	0.1602
	Present	0.0708	0.1268	0.0695	0.1619	0.3397	0.1582
2	S-FSDT based IGA (Yin et al. 2014)	0.0557	0.1018	0.0548	0.1272	0.2729	0.1245
	Levy (Mohammadi et al. 2010)	0.0557	0.1019	0.0548	0.1272	0.2729	0.1245
	Present	0.0552	0.0989	0.0542	0.1264	0.2651	0.1235
(b) SSSS							
1	S-FSDT based IGA (Yin et al. 2014)	0.7429	0.3571	0.2472	0.6846	0.6846	0.3423
	Levy (Mohammadi et al. 2010)	0.7430	0.3572	0.2473	0.6848	0.6848	0.3424
	R-STSDT-MK (Vu et al. 2018)	0.7478	0.3577	0.2477	0.6850	0.6850	0.3425
	Present	0.7398	0.3412	0.2361	0.6695	0.6695	0.3347
2	S-FSDT based IGA (Yin et al. 2014)	0.5797	0.2787	0.1929	0.5342	0.5342	0.2671
	Levy (Mohammadi et al. 2010)	0.5798	0.2787	0.1930	0.5343	0.5343	0.2672
	R-STSDT-MK (Vu et al. 2018)	0.5838	0.2791	0.1933	0.5346	0.5346	0.2673
	Present	0.5325	0.2663	0.1843	0.5225	0.5225	0.2613
(c) SCSC							
1	S-FSDT based IGA (Yin et al. 2014)	1.2177	0.8622	0.6448	1.3161	1.1542	0.6554
	Levy (Mohammadi et al. 2010)	1.2181	0.8622	0.6450	1.3167	1.1544	0.6556
	R-STSDT-MK (Vu et al. 2018)	1.2167	0.8649	0.6455	1.3224	1.1694	0.6579
	Present	1.2200	0.8684	0.6467	1.3048	1.1538	0.6489
2	S-FSDT based IGA (Yin et al. 2014)	0.9502	0.6728	0.5031	1.0270	0.9006	0.5114
	Levy (Mohammadi et al. 2010)	0.9506	0.6728	0.5033	1.0274	0.9008	0.5116
	R-STSDT-MK (Vu et al. 2018)	0.9511	0.6758	0.5045	1.0342	0.9145	0.5142
	Present	0.9541	0.6783	0.5050	1.0200	0.9010	0.5070

$$\sigma_x^0 = \zeta_1 p \quad \sigma_y^0 = \zeta_2 p \quad \tau_{xy}^0 = 0 \qquad (38)$$

where p is the applied load per unit length, while ζ_1, ζ_2 are the load parameters signified the loading condition. Negative values of the load parameter indicate compression, and vice versa.

4.4.1 Isotropic FGM plates (type A)

In this example, the buckling analysis of an isotropic FGM plate with various boundary conditions made from Al/Al$_2$O$_3$ is investigated. The ratios of plate's width to thickness and length to width are respectively $b/h = 100$ and $a/b = 1.5$. Figure 7 plots the first five buckling modes of the Al/Al$_2$O$_3$ free—simply supported square plate with $a/b = 1.5$ and $(\zeta_1 = 0, \zeta_2 = -1)$. The normalized buckling load $\bar{N}_{cr} = \frac{12 N_{cr} a^2 \left(1 - v^2\right)}{E h^3}$ of the plate is calculated and compared with the results available in the literature and presented in Table 8. As can be seen in the table, the results derived from the proposed method are in good agreement with the analytical solutions published in literature (Mohammadi et al. 2010). We also compare to a numerical solution based on the IGA (Yin et al. 2014) using S-FSDT, and the MK (Vu et al. 2018) using R-STSDT method.
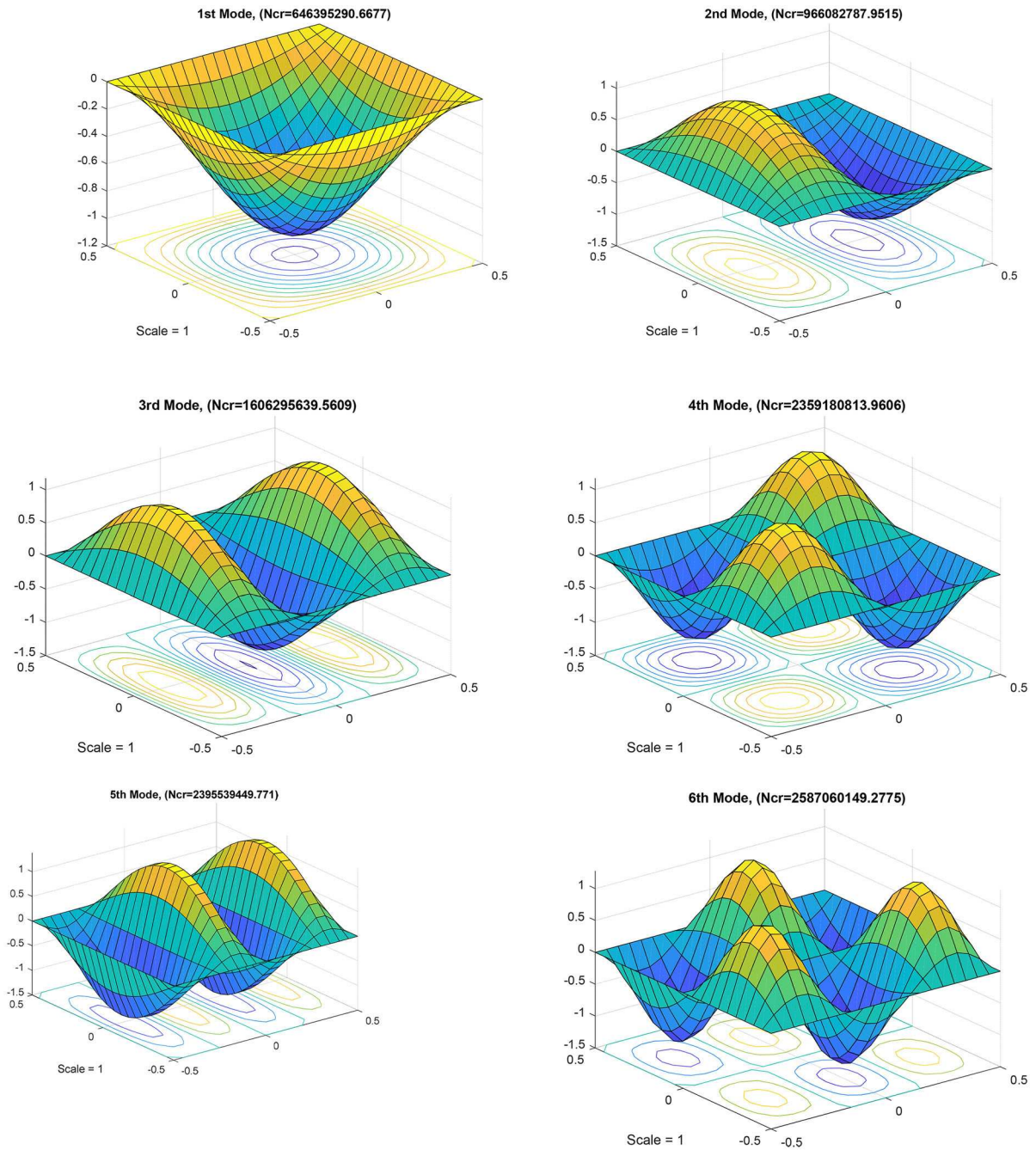
Fig. 8 Plots the first six uni-axial buckling modes of SSSS sandwich FGM plates of Type C with $n = 1.0$ and 1–1–1

It should be noted that the N-RSHSDT gives slightly lower results than those obtained by both S-FSDT based IGA (Yin et al. 2014) and R-STSDT based MK (Vu et al. 2018). Increasing the gradient index decreases the buckling load. Buckling load value is increased from SFSF to SSSS and SCSC since the additional fixity that is posed by the supports. The biaxial in-plane compress loading state has the buckling loads which are lower values than those given by the uni-axial in-plane compress loading state.
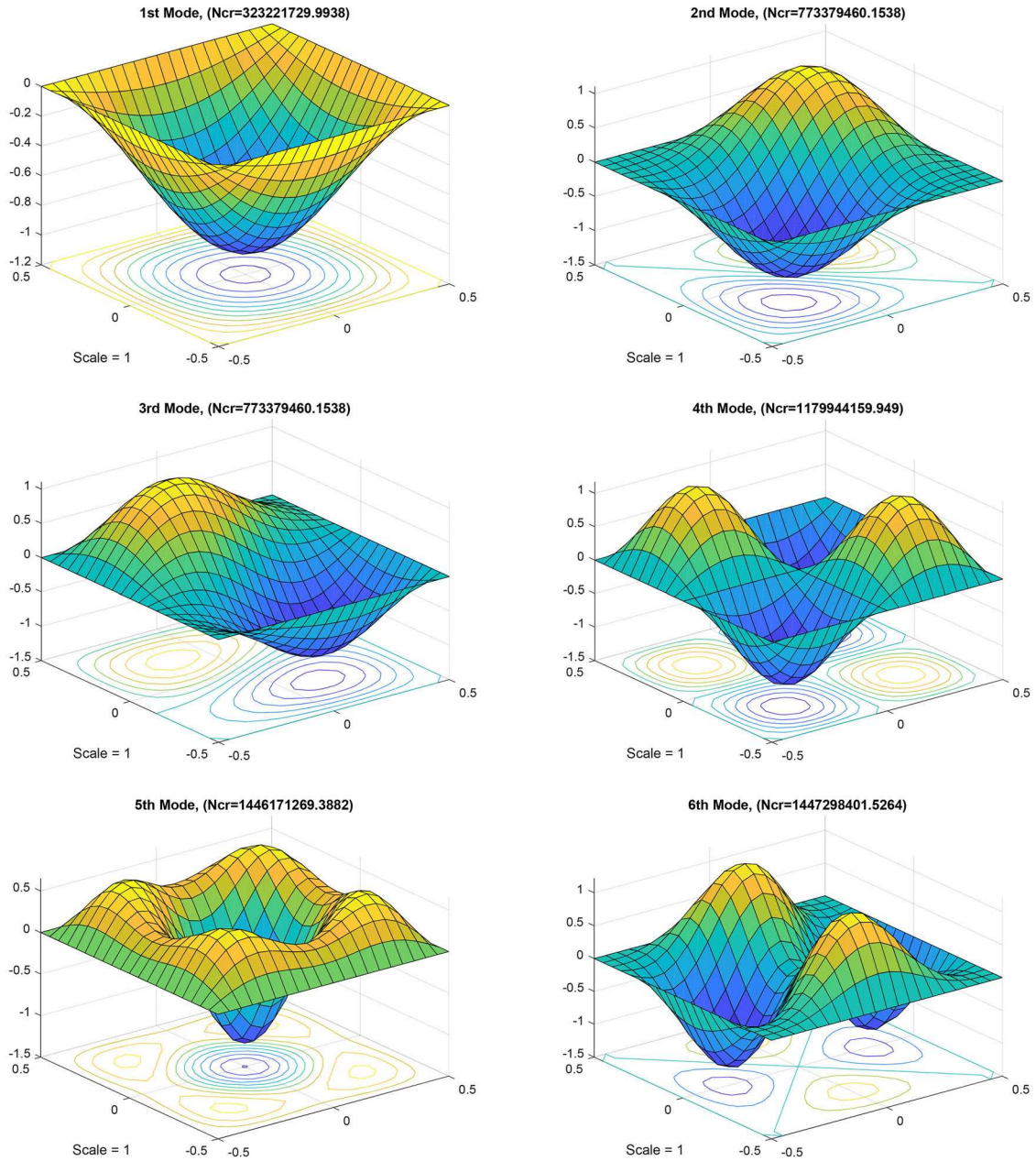
Fig. 9 First six bi-axial buckling modes of SSSS sandwich FGM plates of Type C with $n = 1.0$ and 1–1–1

4.4.2 Sandwich plates with isotropic core and FGM face sheets (type C)

In the problem we examine the normalized critical buckling loads of SSSS sandwich FGM square plate-type C with the thickness ratio $a/h = 10$. The core of the plate is the pure ceramic, while FGM skins are made from the metal-rich at top and bottom surfaces. FGM properties are assumed as $E_c = 380E_0$, $E_m = 70E_0$ with $E_0 = 1$ GPa. Figure 8 plots the first five uni-axial buckling modes of the plate with graded index $n = 1.0$ and layer thickness ratios 1–1–1, while Fig. 9 plots the first five bi-axial buckling modes one

Table 9 The uni-axial critical buckling load of SSSS sandwich FGM plates of Type C with $(a/h = 10)$

n	Method	1–0–1	2–1–2	2–1–1	1–1–1	2–2–1	1–2–1
0.0	SSDT (Zenkour 2005)	13.0061	13.0061	13.0061	13.0061	13.0061	13.0061
	TSDT (Reddy 2000)	13.0050	13.0050	13.0050	13.0050	13.0050	13.0050
	HSDT (Baferani et al. 2011)	12.9529	12.9529	12.9529	12.9529	12.9529	12.9529
	Present	13.0031	13.0031	13.0031	13.0031	13.0031	13.0031
1.0	SSDT (Zenkour 2005)	5.1685	5.8412	6.1946	6.4654	6.9498	7.5063
	TSDT (Reddy 2000)	5.1671	5.8401	6.1939	6.4647	6.9494	7.5066
	HSDT (Baferani et al. 2011)	5.0614	5.7114	6.0547	6.3150	6.7841	7.3200
	Present	5.1676	5.8401	6.1941	6.4640	6.9489	7.5043
5.0	SSDT (Zenkour 2005)	2.6601	3.0441	3.4045	3.5806	4.1129	4.7349
	TSDT (Reddy 2000)	2.6582	3.0426	3.4035	3.5796	4.1121	4.7347
	HSDT (Baferani et al. 2011)	2.6365	3.0079	3.3626	3.5301	4.0507	4.6470
	Present	2.6600	3.0438	3.4055	3.5800	4.1136	4.7336
10.0	SSDT (Zenkour 2005)	2.4893	2.7484	3.1344	3.1946	3.1457	4.3818
	TSDT (Reddy 2000)	2.4873	2.7463	3.0919	3.1947	3.7075	4.2799
	HSDT (Baferani et al. 2011)	2.4722	2.7205	3.0607	3.1576	3.6617	4.2055
	Present	2.4894	2.7479	3.0940	3.1955	3.7095	4.2793

Table 10 The bi-axial critical buckling load of SSSS sandwich FGM plates of Type C with $(a/b = 10)$

n	Method	1–0–1	2–1–2	2–1–1	1–1–1	2–2–1	1–2–1
0.0	SSDT (Zenkour 2005)	6.5030	6.5030	6.5030	6.5030	6.5030	6.5030
	TSDT (Reddy 2000)	6.5025	6.5025	6.5025	6.5025	6.5025	6.5025
	HSDT (Baferani et al. 2011)	6.4764	6.4764	6.4764	6.4764	6.4764	6.4764
	Present	6.5022	6.5022	6.5022	6.5022	6.5022	6.5022
1.0	SSDT (Zenkour 2005)	2.5842	2.9206	3.0973	3.2327	3.4749	3.7531
	TSDT (Reddy 2000)	2.5836	2.9200	3.0970	3.2324	3.4747	3.7533
	HSDT (Baferani et al. 2011)	2.5307	2.8557	3.0273	3.1575	3.3920	3.6600
	Present	2.5840	2.9203	3.0973	3.2322	3.4747	3.7524
5.0	SSDT (Zenkour 2005)	1.3300	1.5220	1.7022	1.7903	2.0564	2.3674
	TSDT (Reddy 2000)	1.3291	1.5213	1.7018	1.7898	2.0561	2.3673
	HSDT (Baferani et al. 2011)	1.3183	1.5040	1.6813	1.7650	2.0254	2.3235
	Present	1.3301	1.5220	1.7028	1.7901	2.0569	2.3670
10.0	SSDT (Zenkour 2005)	1.2448	1.3742	1.5672	1.5973	1.5729	2.1909
	TSDT (Reddy 2000)	1.2436	1.3732	1.5460	1.5974	1.8538	2.1400
	HSDT (Baferani et al. 2011)	1.2361	1.3602	1.5303	1.5788	1.8308	2.1028
	Present	1.2448	1.3740	1.5471	1.5979	1.8549	2.1398

for case of graded index $n = 1.0$ and layer thickness ratios 1–1–1.

The normalized critical load has a form as follow $\bar{N}_{cr} = \frac{N_{cr}a^2}{100E_0h^3}$. The critical buckling loads predicted by the present approach are tabulated in Tables 9 and 10 for various power-law exponents n and layer thickness ratios. Both tables include results obtained from Zenkour's sinusoidal shear deformation plate theory SSDT(Zenkour 2005), Reddy's higher-order shear deformation plate theory TSDT (Reddy 2000) and quasi-3D higher-order shear deformation theory HSDT(Baferani et al. 2011).

Table 9 indicated the uni-axial critical buckling load, while Table 10 indicated the bi-axial critical buckling load. It is clear that a good agreement between the present references solution. This allow us to conclude that new refined sin hyperbolic shear deformation plate theory is good for modelling of simply supported sandwich FGM plates and that the new multi-quadric correlation function is a good formulation.

It is worth nothing that the case of isotropic fully ceramic plate (first row on Tables 9, 10) has the highest values of critical buckling load. Furthermore, the critical buckling loads increase as the ratio of the core to total thickness of plate ($[z_3 - z_2]/h$) increase. As can be seen in tables, we may conclude that the critical buckling loads decrease when the gradient indices increase, also, it is observed that the uni-axial buckling load is double the bi-axial one for the sandwich FGM.

5 Conclusions

This work presents a novel computational approach based on a combination of four variable refined formulation and moving Kriging interpolation method for static bending, free vibration and buckling analyses of isotropic and sandwich composite FGM plates. In the present model, a new sin hyperbolic distribution function representing the transverse shear strains through the plate thickness was proposed. Using this framework, the proposed model reduces the computational cost when compared to the traditional TSDT or HSDT models. Shear correction factor is not required, since the proposed model naturally satisfies shear stress free conditions at the top and bottom surfaces of the plates. Furthermore, a new multi-quadric correlation function in terms of the moving Kriging interpolation method is proposed to eliminate classical drawbacks and provides a stable solution. Results for both thin to thick, isotropic to sandwich FGM plates with various values of the gradient index and boundary conditions correlated excellently with available solution from the literature showing the high reliability of the present method.

References

Baferani, A.H., Saidi, A.R., Jomehzadeh, E.: An exact solution for free vibration of thin functionally graded rectangular plates. Proc. Inst. Mech. E Part C J. Mech. Eng. Sci. **225**(C3), 526–536 (2011)

Bessaim, A., Houari, M.S.A., Tounsi, A., Mahmoud, S.R., Adda Bedia, E.A.: A new higher-order shear and normal deformation theory for the static and free vibration analysis of sandwich plates with functionally graded isotropic face sheets. J. Sand. Struct. Mater. **15**, 671–703 (2013)

Bui, Q.T., Nguyen, N.M.: A moving Kriging interpolation-based meshfree method for free vibration analysis of Kirchhoff plates. Comput. Struct. **89**, 380–394 (2011)

Bui, Q.T., Nguyen, N.T., Nguyen, D.H.: A moving Kriging interpolation-based meshless method for numerical simulation of Kirchhoff plate problems. Int. J. Numer. Meth. Eng. **77**, 1371–1395 (2009)

Bui, Q.T., Nguyen, N.M., Zhang, Ch.: An efficient meshfree method for vibration analysis of laminated composite plates. Comput. Mech. **48**, 175–193 (2011)

Bui, Q.T., Doan, H.D., Do, V.T., Hirose, S., Nguyen, D.D.: High frequency modes meshfree analysis of Reissner-Mindlin plates. J. Sci. Adv. Mater. Dev. **1**, 400–412 (2016)

Carrera, E., Brischetto, S.: Analysis of thickness locking in classical, refined and mixed multilayered plate theories. Compos. Struct. **82**, 549–562 (2008a)

Carrera, E., Brischetto, S.: Analysis of thickness locking in classical, refined and mixed theories for layered shells. Compos. Struct. **85**, 83–90 (2008b)

Carrera, E., Brischetto, S., Cinefra, M., Soave, M.: Effects of thickness stretching in functionally graded plates and shells. Compos. Part B Eng. **42**(2), 123–133 (2011)

Chen, J.S., Hillman, M., Chi, S.W.: Meshfree methods: progress made after 20 years. J. Eng. Mech **143**, 04017001 (2017)

Do, V.T., Bui, Q.T., Yu, T.T., Pham, T.D., Nguyen, T.C.: Role of material combination and new results of mechanical behavior for FG sandwich plates in thermal environment. J. Comput. Sci. **21**, 164–181 (2017)

Ha, H.K.: Finite element analysis of sandwich plates: an overview. Comput. Struct. **37**, 397–403 (1990)

Lee, Y.Y., Zhao, X., Liew, K.M.: Thermoelastic analysis of functionally graded plates using the element-free kp-Ritz method. Smart Mater. Struct. **18**(3), 35007 (2009)

Li, Q., Iu, V.P., Kou, K.P.: Three-dimensional vibration analysis of functionally graded material sandwich plates. J. Sound Vib. **311**, 498–515 (2008)

Mohammadi, M., Saidi, A., Jomehzadeh, E.: Levy solution for buckling analysis of functionally graded rectangular plates. Appl. Compos. Mater. **17**, 81–93 (2010)

Neves, A.M.A., Ferreira, A.J.M., Carrera, E., Cinefra, M., Jorge, R.M.N., Soares, C.M.M.: Static analysis of functionally graded sandwich plates according to a hyperbolic theory

considering Zig-Zag and warping effects. Adv. Eng. Softw. **52**, 30–43 (2012)

Neves, A.M.A., Ferreira, A.J.M., Carrera, E., Cinefra, M., Roque, C.M.C., Jorge, R.M.N.: Static free vibration and buckling analysis of isotropic and sandwich functionally graded plates using a quasi-3D higher-order shear deformation theory and a meshless technique. Compos. Part B Eng. **44**, 657–674 (2013)

Reddy, J.N.: Analysis of functionally graded plates. Int. J. Numer. Methods Eng. **47**, 663–684 (2000)

Sadamoto, S., Tanaka, S., Taniguchi, K., Ozdemir, M., Bui, Q.T., Murakami, C., Yanagihara, D.: Buckling analysis of stiffened plate structures by an improved meshfree flat shell formulation. Thin Walled Struct. **117**, 303–313 (2017)

Vu, T.V., Phan, V.S.: A modified moving Kriging interpolation-based meshfree method with refined sinusoidal shear deformation theory for analysis of functionally graded plates. In: Proceedings of the International Conference on Advances in Computational Mechanics, pp. 485–501 (2017)

Vu, T.V., Nguyen, N.H., Khosravifard, A., Hematiyan, M.R., Tanakad, S., Bui, T.Q.: A simple FSDT-based meshfree method for analysis of functionally graded plates. Eng. Anal. Bound. Elem. **79**, 1–12 (2017)

Vu, T.V., Khosravifard, A., Hematiyan, M.R., Bui, T.Q.: A new refined simple TSDT-based effective meshfree method for analysis of through-thickness FG plates. Appl. Math. Model. **57**, 514–534 (2018)

Yaghoobi, H., Yaghoobi, P.: Buckling analysis of sandwich plates with FGM face sheets resting on elastic foundation with various boundary conditions: an analytical approach. Meccanica **48**, 2019–2035 (2013)

Yin, S.H., Yu, T.T., Liu, P.: Free vibration analyses of FGM thin plates by isogeometric analysis based on classical plate theory and physical neutral surface. Adv. Mech. Eng. ArticleID 634584 (2013)

Yin, S.H., Jack, S.H., Yu, T.T., Bui, Q.T., Boras, P.A.S.: Iso-geometric locking-free plate element: a simple first order shear deformation theory for functionally graded plates. Compos. Struct. **118**, 121–138 (2014)

Zenkour, A.M.A.: Comprehensive analysis of functionally graded sandwich plates: part 2 buckling and free vibration. Int. J. Solids Struct. **42**, 5243–5258 (2005)